A Practical Microcylinder Appearance Model for Cloth Rendering

IMAN SADEGHI
OLEG BISKER
JOACHIM DE DEKEN
HENRIK WANN JENSEN
UC San Diego

This paper introduces a practical shading model for cloth that can simulate both anisotropic highlights as well as the complex color shifts seen in cloth made of different colored threads. Our model is based on extensive Bidirectional Reflectance Distribution Function (BRDF) measurements of several cloth samples. We have also measured the scattering profile of several different individual cloth threads. Based on these measurements we have derived an empirical shading model capable of predicting the light scattered by different threads. We model cloth as a collection of threads in a weave pattern, which provides a description about the coverage of the different thread types as well as their tangent directions. Our model accounts for shadowing and masking by the threads. We validate our model by comparing predicted and measured values and we show how it can reproduce the appearance of different cloth samples with complex structure including silk, velvet, linen, and polyester. Our model is robust, easy to use, and it can model cloth types with complex highlights and color shifts that cannot be handled by previous models.

1. INTRODUCTION

Cloth is a complex material made of interwoven threads of different types. Its appearance can vary from matte diffuse to highly specular and anisotropic. Existing models for simulating the appearance of cloth are either too simplistic to produce a faithful rendering, or too complex for practical use.

In this paper we present a practical appearance model for cloth. Our model is based on extensive measurements of light scattering by cloth samples and individual threads. Based on these measurements, we have developed a robust empirical shading model for woven cloth based on light scattering from individual threads. Our appearance model simulates distant viewing of cloth and ignores the appearance of individual threads unlike recent work on fabrics [Irawan and Marschner 2012]. Our model takes into account shadowing and masking that occurs between neighboring threads. It is easy to control and can reproduce a wide range of fabrics including those made of linen, silk, polyester, and velvet (see Figure 1). We provide measured parameters for these cloth types including the weave definitions for our cloth samples (Figure 2).

The main advantage of our model is that it takes intuitive parameters that are fabric specific. The parameters are derived from naked eye observation of the weave pattern, as well as the constrained parametric space of our analytical thread scattering function. This enables the model to describe fabric BRDFs with or without measurements of a real cloth sample. Unlike a general microfacet model, which abstracts surface microstructure as a distribution of normals, our model allows for explicit control of the color and shininess of individual threads and precise definition of the weave structure.
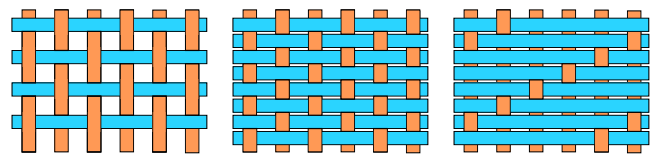

Fig. 2: Different weaving patterns of the fabrics studied in this paper: (left) Plain, (middle) Crepe de Chine, and (right) Satin Charmeuse.

2. PREVIOUS WORK

Rendering cloth has been an active area of research for more than 25 years. The earliest approaches as well as more recent work are based on simple empirical shading models [Weil 1986; Daubert et al. 2001; Glumac and Doepp 2004], where the primary goal is to achieve believable shading rather than physical accuracy. Microfacet models have been used by Ashikhmin et al. to model satin and velvet [Ashikhmin et al. 2000]. Adabala et al. continued this work by including support for weave patterns [Adabala et al. 2003]. Wang et al. [2008] introduced their own microfacet-based BRDF for modeling spatially-varying anisotropic reflectance using data
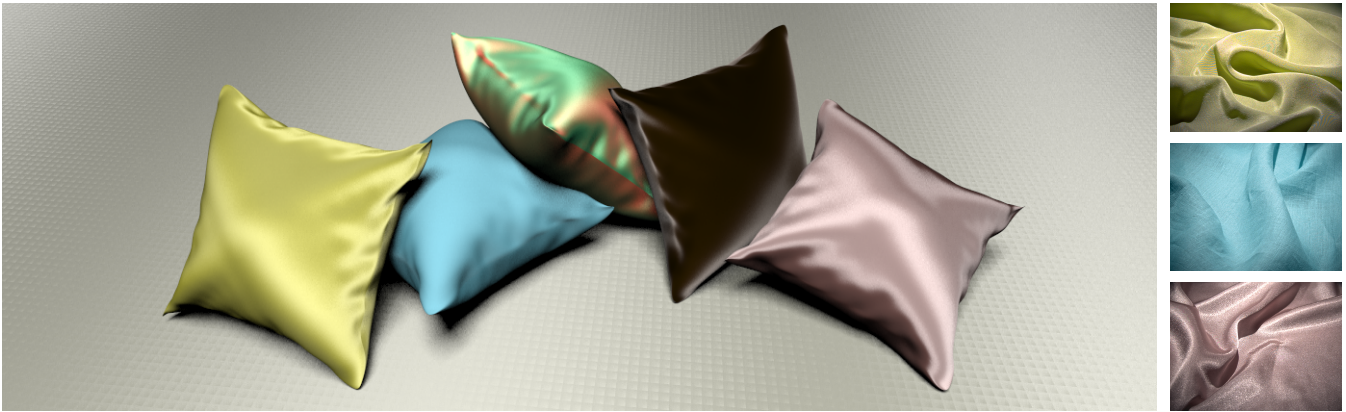
Fig. 1: Image rendered using our cloth shading model for different fabric types. Left to right the fabrics are: Silk Crepe de Chine, Linen Plain, Silk Shot Fabric, Velvet, and Polyester Satin Charmeuse. (right) Reference photos for three of the fabrics rendered.

captured from a single view. While microfacet models can be effective at capturing a complex appearance these models are difficult to control as they depend strongly on the right normal distribution function. Since cloth is often anisotropic, it is difficult to obtain this distribution from measured data (see Section 7).

Another approach for simulating cloth is based on modeling the structure of the cloth [Xu et al. 2001; Chen et al. 2003; Drago and Chiba 2004; Schröder et al. 2011]. While these methods can reproduce a wide range of appearances they can be difficult to control. Yasuda et al. [1992] modeled the gloss seen in cloth by accounting for the internal structure, but assumed a highly simplified model of the cloth surface and the results lacked verification. Westin et al. [1992] computed BRDFs for velvet and plain weave nylon fabrics by ray tracing a geometric model of the small-scale cloth structure. Zhao et al. [2011] presented a volumetric rendering approach using CT scanning of cloth fabrics. Their model produces high quality renderings but is limited to reproducing cloth samples measured with a sophisticated measurement device.

Irawan et al. developed a comprehensive model for reproducing both the small-scale (BTF) and large-scale (BRDF) appearance of woven cloth [Irawan and Marschner 2012]. This model is current state of the art and capable of reproducing a wide range of appearances. It is an empirical model based on light interaction with thread fibers. This model is evaluated numerically to fit with measured data. The numerical fit is rather costly and to reduce the number of parameters in the model only a limited set of thread directions (only hyperbolic curves) can be accounted for. This limits the accuracy of the model as it cannot reproduce more than two specular highlights. Furthermore, the model does not account for shadowing and masking between different threads, which limits the accuracy at grazing angles. We compare our model to Irawan's model and show how we are able to match measured cloth samples more accurately in addition to handling the assymetric highlights in Velvet and the multiple highlights present in the Polyester Satin Charmeuse.

3. LIGHT SCATTERING FROM FABRICS

3.1 Acquisition Setup

The cloth measurements presented in this paper were acquired with a fully automatic, four-axis image-based gonioreflectometer at UC San Diego. The device consists of two robotic arms, each with two degrees of freedom. Each degree of freedom has a minimum

displacement of 0.1 degrees, allowing the arms to move freely to nearly any desired position on the sphere which surrounds the measurement platform. Data capture is enabled by mounting a CCD camera on the outer arm and a light source on the inner arm. In addition to quantitative analysis of cloth reflectance, we investigated different fabric types and their constituent threads under a microscope to gain further intuition about their behavior. We have measured two perpendicular 2D BRDF slices for each fabric and full 3D BRDF measurements for cloth threads (Section 4).

3.2 BRDF Measurements and Observations

The BRDF measurements in this section have been acquired by placing the light source and camera in-plane, perpendicular to the fabric sample. Each BRDF plot represents a fixed incident light angle and a continuous range of camera angles. Our measurements show that the appearance of cloth is dominated by some combination (in varying amounts) of diffuse reflectance, specular reflectance, shadowing/masking, and grazing angle sheen. While many samples were measured, we focused on three fabrics: Linen Plain, Silk Crepe de Chine, and Polyester Charmeuse. Since each fabric has a unique combination of fiber type, thread structure, and weaving pattern, their measurements provide insight into which physical characteristics are responsible for the variation in their appearance. The resulting set of observed light scattering behaviors produced by these fabrics have not previously been fully addressed in literature nor have they been validated with ample physical measurements.

3.2.1 *Linen Plain.* The measured Linen sample is a plain weave fabric assembled with a single type of thread. This particular construction causes the material to look the same both front and back, as well as from orthogonal viewing directions. Under the microscope, as shown in Figure 3a, we observe a repeating grid of twisted threads. Due to its orthogonally symmetric structure, linen was measured along one direction. Figure 4 shows the normal plane BRDF measurements of this fabric along one of its threads. The orange line indicates the direction of incident light. The gaps in the plots are due to the occlusion of the light source by the camera. The measurements confirm that linen produces a smooth reflection with no specular peaks under most lighting conditions, except when the fabric is observed at a grazing angle and the light is also grazing. As seen in Figure 4 (right), at these grazing angles, reflectance increases substantially. The measurements also show that the effect
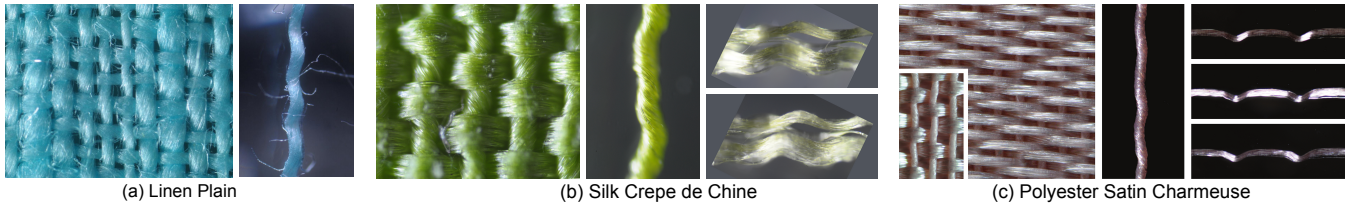
(a) Linen Plain   (b) Silk Crepe de Chine   (c) Polyester Satin Charmeuse

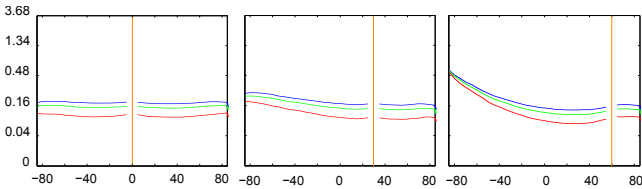Fig. 3: Close-ups taken with a microscope of different fabrics and threads.

Fig. 4: BRDF measurements for Linen Plain for 0°, 30°, and 60° incident angles.

of shadowing/masking, manifested by dips at the plot edges, is minimal.

3.2.2 *Silk Crepe de Chine.* The measured Silk Crepe de Chine sample is assembled with two different types of threads (Figure 3b). The first type of thread is made of densely twisted fibers. This thread remains straight and uniformly spaced in the fabric. The second type of thread is made of thin and untwisted fibers, and passes above and below the first type. This thread exhibits sharp surface reflection and very little absorption resulting in its translucent appearance. While moving a light around the microscope, a strong specular reflection in two incidence directions is visible. The variation in thread type as well as the weaving pattern structure result in an asymmetrical surface which causes this fabric to appear significantly different depending on viewing direction. To study this, we measured the fabric BRDF along two orthogonal directions (Figure 5). Measurements in the plane parallel to the flat threads (top row) show two off-specular peaks, while the perpendicular plane measurements (bottom row) exhibit two grazing angle peaks. Furthermore, the parallel measurements clearly indicate a drop in reflectance as the eye approaches grazing angle, suggesting the contribution of shadowing/masking. In contrast, the perpendicular measurements maintain the grazing angle peaks under all lighting conditions.
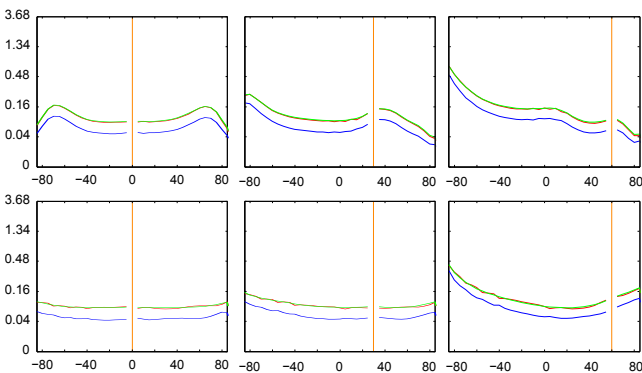

Fig. 5: BRDF measurements for Silk Crepe de Chine for 0°, 30°, and 60° incident angle. The top row corresponds to the in plane measurements parallel to the direction of flat threads, and the bottom row represents the measurements in the perpendicular direction.

3.2.3 *Polyester Satin Charmeuse.* The measured Polyester Satin Charmeuse sample is a satin weave fabric, meaning that the threads in one direction cross over most of the threads in the other direction. Like Silk, this fabric is made out of two distinct (polyester) threads. The flat threads go above and below the twisted threads, but remain longer above than below. This asymmetry in the weaving pattern causes the fabric to have two different sides (Figure 3c). While moving the light around the microscope, we noticed strong reflections in three different direction of light. The variation in thread type and the asymmetric weaving pattern result in strong anisotropic scattering. The fabric was measured in two perpendicular planes (Figure 6). In plane measurements along the direction of flat threads exhibit three specular peaks, one in the reflection direction and the other two in equal but opposite off-specular directions. Measurements in the perpendicular plane exhibit grazing angle peaks which are visible under all lighting conditions.
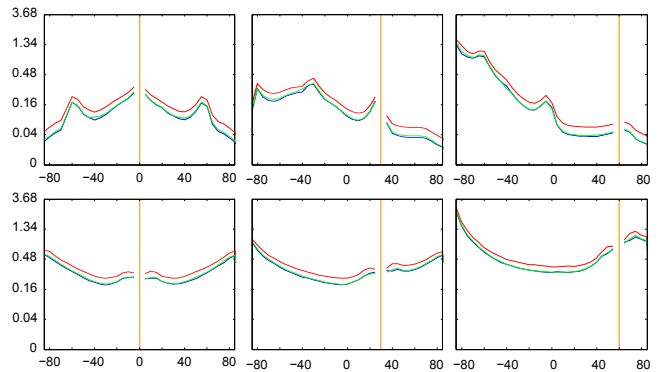

Fig. 6: BRDF measurements for Polyester Charmeuse for 0°, 30°, and 60° incident angles. Top row corresponds to in plane measurements along the direction of flat threads, and the bottom row represents measurements in the perpendicular direction.

4.   LIGHT SCATTERING FROM THREADS

In the previous section we noted that the there are two different types of threads that contribute to the overall appearance of fabrics. The first and most common type of threads are densely twisted threads. These threads have many varieties that differ by twist level and constituent fiber count. The twist level of threads affects the compactness and density of fibers that compose them [Saville 1999]. The second type of threads have a minimal amount of twist in their construction and we refer to them as flat threads. These are usually less dense and have a greater diameter due to their loosely packed structure. Both thread categories are fed by a diverse selection of raw materials such as silk, cotton, wool, flax, and synthetic filaments. We further investigate the light scattering properties of cloth by measuring the BSDF of different types of threads.

4.1 Acquisition Setup

We measured the scattered radiance distribution of several thread types using the same spherical gantry as used for the cloth measurements and a unique suspension apparatus. The results serve to validate our analytical model as well as provide a qualitative basis for reasoning about threads and cloth in general. In our measurements we illuminate an 8 cm section of thread with a collimated light beam and collect radiance scattering measurements with a CCD camera.

Fig. 7: The gantry setup used to measure the BSDF of threads. The thread is suspended vertically, which makes it possible to capture the full 4D BSDF.

To procure a thread sample, we first remove a single strand from a finished fabric. When a thread is removed from fabric it is no longer straight, but retains the shape that it had in the fabric. In order to obtain accurate scattering measurements, the thread must be extended to its maximal length. This type of procedure is common in fabric quality testing and requires standard tension, which has the general goal of non-destructively pulling on one end of the thread. In our experimental thread mount, we clamp one end of the thread to a poseable arm, and let the rest of it hang, weighed down by a magnetic set of spheres at the unclamped end. Hanging the thread in mid-air allows the gantry to measure a full 4D BSDF with minimal occlusions and no background to contaminate the measurements (see Figure 7). Additionally, gravity provides a consistent vertically-aligned axis, which eliminates the need for pose calibration.

4.2 BSDF Measurements

We measured a 3D BSDF by varying the longitudinal angles θ_i, θ_r, and the azimuthal difference angle $\phi_d = \phi_i - \phi_r$. Figure 9 shows the notations used in our paper. We did not measure a 4D BSDF because we assumed symmetry of the BSDF with respect to ϕ. Since threads are not perfect cylinders, this assumption is somewhat violated, however, it allows us to capture less data while still observing the salient thread scattering features. We present a planar slice of the resulting measurements in Figure 8. Here the BSDF is a function of two angles θ_i and θ_r). We present several θ_i angles and plot a continuous range of BSDF measurements for θ_r. The threads were not treated with any dyes and no polarizing filters were used. As a result, the BSDF plots represent the naturally visible combination of surface reflection and internal scattering. To facilitate intuition about the plots we can state the following: surface reflection results in a lobe in the specular reflection direction ($\theta_r = -\theta_i$), and internal scattering results in a wider lobe that is more decoupled from appearing in the specular direction. The top row of Figure 8
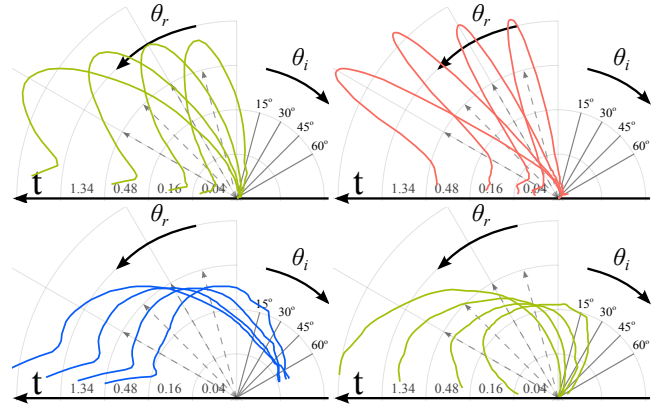

Fig. 8: Polar plots of measured incidence plane BSDF for different threads. Each quadrant of the figure contains the RGB average BSDF for a thread type. Starting at the top row, and moving left to right we have flat silk thread, flat polyester thread, twisted linen thread, and twisted silk thread.

demonstrates the similarity among flat threads and their disparity from twisted threads. In the top row, both the polyester and the silk thread possess narrow specular lobes oriented at the exact specular reflection direction. This result can be attributed to their low surface roughness as well as minimal internal scattering. The fact that the lobe is oriented at the exact specular reflection direction means that, unlike hair, threads have no consistent cuticle that displaces their specular reflection. The polyester thread is the more specular of the two flat threads, as evidenced by its narrower and brighter reflection lobe. This can be attributed to the synthetic vs. organic fibers that they are composed of, where polyester has fewer natural imperfections and irregularities due to its industrial fabrication process.

At first glance the twisted threads in the bottom row of Figure 8 appear nearly identical. They both exhibit a characteristic wide scattering lobe that slowly increases as the light goes to glancing angle. Focusing on glancing incidence angles, we observe that the twisted linen thread scatters more light in the non-specular directions. This type of scattering can be attributed to either a very rough surface or isotropic internal scattering. We address these behaviors in subsequent sections when we present our thread BSDF model.
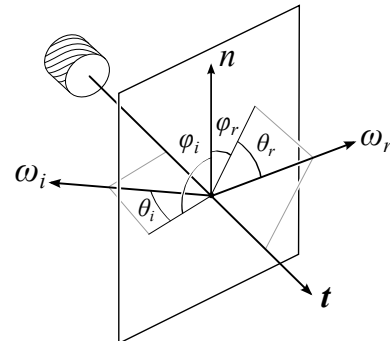

Fig. 9: Notations and geometry of light reflection from a cylindrical fiber. Longitudinal angles θ are computed with respect to the normal plane and the azimuthal angles ϕ are computed based on the local surface normal direction n. When the thread is not part of a fabric n can be any arbitrary direction within the normal plane.

4.3 A Light Scattering Model for Threads

Based on our measurements of individual threads, we observed an optical behavior that is similar to hair and more generally, smooth dielectric cylinders. We observed that the reflection of a collimated light beam from a taut thread sample forms a cone centered on the thread axis. Additionally, the surface reflection is framed by a subtle color reflection that is also centered at the cone. This type of reflection from cylinders has been previously studied by [Kajiya and Kay 1989; Kim 2002; Marschner et al. 2003], where the normal plane around the tangent is used as the coordinate frame for computing light scattering behavior. Unlike hair, threads do not have consistent tilted cuticles on their surface and therefore the reflected rays are distributed around the reflection cone. In our model we

f_s	Thread scattering function
F_r	Fresnel reflectance
F_t	Fresnel transmittance
γ_s	Surface reflectance Gaussian width
γ_v	Volume scattering Gaussian width
k_d	Isotropic scattering coefficient
A	Colored albedo coefficient

Table I. : Description of important symbols.

use the cylinder abstraction to represent a thread. When an incident beam from ω_i consisting of parallel rays of light strikes a thread cylinder running along the vector t, each ray in the beam reflects at the surface according to the surface normal of the cylinder. These surface normals are all perpendicular to the thread tangent vector t and lie in the normal plane. For a smooth specular cylinder, a beam incident at θ_i will be reflected in the ideal specular direction $-\theta_i$ across the normal plane and, due to the circular cross section of the cylinder, will be spread into a cone [Kajiya and Kay 1989]. The refracted light will enter the cylinder and after any number of internal reflections and refraction will emit into the same cone as the surface specular reflection [Marschner et al. 2003].

To establish radiometric notation for our cylinder based model we use the curve radiance integral from [Marschner et al. 2003]:

$$L_r = \int f_s(t, \omega_i, \omega_r) L_i(\omega_i) \cos \theta_i \, d\omega_i \qquad (1)$$

Note that unlike the standard radiance integral on a surface, the reflected radiance from a cylinder differs by the fact that it is defined over a unit length instead of a unit area. This difference arises from the fact that the cylinder scattering function accounts for all the light scattered around the circumference of the cylinder.

As in previous treatments of BSDFs [Hanrahan and Krueger 1993], we separate our scattering function $f_s(t, \omega_i, \omega_r)$ into a surface scattering component $f_{r,s}$, and volume scattering component $f_{r,v}$. In addition to the angles in Figure 9, we introduce $\phi_d = \phi_i - \phi_r$, $\theta_h = (\theta_i + \theta_r)/2$, and $\theta_d = (\theta_i - \theta_r)/2$ to define the two scattering functions.

4.3.1 Surface Reflection.
We model surface reflection similarly to [Marschner et al. 2003], except we do not decompose our computation into longitudinal and azimuthal planes.

$$f_{r,s}(t, \omega_i, \omega_r) = F_r(\eta, \vec{w_i}) \cos(\phi_d/2) g(\gamma_s, \theta_h) \qquad (2)$$

The $\cos(\phi_d/2)$ term arises due to projection of the circular cylinder cross-section, as demonstrated by [Kim 2002], and previously used by [Sadeghi et al. 2010] for hair rendering. To break away from the idealized smooth cylinder representation of threads, we

employ a unit area Gaussian g with width γ_s to simulate surface roughness. Finally, we add a physical basis to the model by attenuating the power by a Fresnel term. The angle used to compute the Fresnel term is based on the reflection normal on the cylinder as well as a half-angle between the light and the eye, yielding an exact expression $F_r(\eta, \cos^{-1}(\cos(\theta_d)\cos(\phi_d/2)))$. Here, θ_d comes from the effective angle between our incident light and the ideally oriented facet to result in a reflection toward the view direction. The ϕ_d angle arises from the fact that we are modeling a cylinder and the ideal reflection between the light and the view direction is also dependent on the azimuthal difference angle. This model produces a glossy reflection on a cone around the thread with physical and geometric attenuation. We considered using the full microfacet specular formulation, but found that it did not improve the matching to our measured results.

4.3.2 Volume Scattering.
Real threads are composed of fibers that are either twisted together or lay flat next to each other. We make a unifying assumption that all fiber types are cylindrical with minimal eccentricity. This is generally true with the exception of cotton, which resembles a flat ribbon. To summarize, our model is a large thread cylinder composed of tiny fiber subcylinders. This enables us to use the fact that smooth cylinders emit light due to surface and internal scattering into the ideal reflection cone. Therefore, light that enters the thread volume and undergoes any type of scattering interaction with the fiber subcylinders will result in a surface emission distributed around the same cone as the surface reflection. This scattering property is very important because it implies that internal scattering can be anisotropic. From our thread BSDF measurements, we found that grazing angle illumination of threads produced varying degrees of colored forward scattering. One thing to note is that the orientation of the fiber subcylinders deviates from that of the thread cylinder. We model this deviation as a Gaussian distribution centered on the thread tangent:

$$f_{r,v}(t, \omega_i, \omega_r) = F \frac{(1 - k_d) \, g(\gamma_v, \theta_h) + k_d}{\cos \theta_i + \cos \theta_r} \, A \qquad (3)$$

Here $F = F_t(\eta, \vec{w_i}) F_t(\eta', \vec{w_r'})$ is the product of two transmission Fresnel terms. We define the subcylinder tangent deviation with a Gaussian lobe g with width γ_v. The Gaussian lobe controls the width of the forward scattering cone. For twisted threads, which consist of fibers that deviate from the thread tangent direction, this Gaussian is wider than for flat threads which mainly consist of parallel filaments. Additionally, we define a tunable isotropic scattering term k_d and a color albedo term A. We added an isotropic scattering term to account for cellulose based fibers such as cotton and linen, which predominantly yield isotropic volume scattering instead of a forward scattering cone. The division by the sum of projected cosines comes from Chandrasekhar [1960], in his derivation for diffuse reflectance due to multiple scattering in a semi-infinite medium. Adding this normalization term gave us better matches with our measured results. The complete thread scattering model is a sum of the surface and volume components:

$$f_s(t, \omega_i, \omega_r) = \big(f_{r,s}(t, \omega_i, \omega_r) + f_{r,v}(t, \omega_i, \omega_r)\big)/\cos^2 \theta_d \quad (4)$$

Note that the complete scattering formulation contains a division by $cos^2 \theta_d$, which is necessary to account for the solid angle attenuation of the specular cone [Marschner et al. 2003]. Previous work has addressed volume scattering in threads with a cylindrical phase function in [Irawan and Marschner 2012] as well as the Henyey-Greenstein phase function in [Adabala et al. 2003]. We experimented with various phase functions as well, but found them inadequate due to their decoupled behavior from the direction of
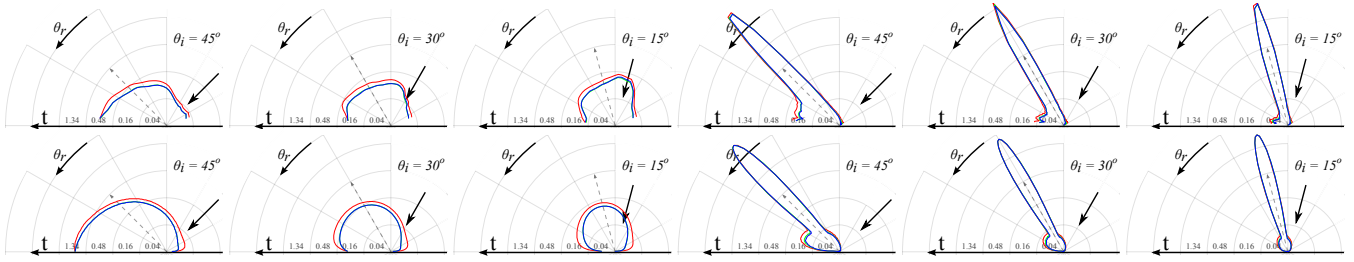
Fig. 10: Incidence plane thread BSDF measurements in the top row matched by thread model in the bottom row. In each row the first three plots are for a twisted thread and the last three for a flat thread. The two threads were extracted from the same Polyester Satin Charmeuse cloth sample. The plots show scattering as a function of view angle.

the thread. Our approach is similar in spirit to [Jakob et al. 2010], which defines phase functions oriented to the direction of fibers to achieve highly anisotropic volume scattering.

We have defined a complete BSDF for individual threads, which matches well to our measured results. It was our goal to define as few non-physical control parameters as possible to enable the model behavior to be driven by physical and geometric scattering constraints. We note that the model is only suitable for distant viewing of threads since it assumes that the rays of light incident on the thread cylinder are parallel and that the thread is locally straight.

4.4 Matching Measured BSDFs

In this section we provide evidence for the validity of our model by comparing it to measured BSDFs of thread. We accomplish this by manually fitting our model parameters to measured results. We did not consider automatic fitting approaches due to the small number of control parameters and their predictable nature.

In Figure 10, we compare the results of our model with measured BSDF results. Each plot shows colored scattering with respect to RGB channels. The per-channel plots demonstrate the whiter color around the specular peak as well as allow us to demonstrate the anisotropic volume scattering term which takes on the albedo color of the thread. Each row shows BSDF measurements for three incident light angles of two thread types: one twisted, and one flat. The first three plots in each row correspond to a twisted polyester thread extracted from the Polyester Satin Charmeuse cloth sample. Our model results in the bottom row are able to closely match the measured results in the top row. We achieve this close fit by observing a wide (rough) surface reflectance Gaussian supplemented by an even wider volume Gaussian and a red tinted albedo coefficient. Note the lack of a clearly identifiable specular lobe as well as a complex forward scattering profile.

The second set of three plots in Figure 10 correspond to a flat polyester thread from the same cloth sample. Our model closely simulates the scattering profile of this thread by setting a very narrow surface reflectance Gaussian and a small red tinted albedo. In these plots we can see a clear separation of a colored forward scattering lobe and an uncolored specular lobe. Our model is validated by being able to closely simulate the scattering behavior of different thread types under various incident light angles.

5. AN APPEARANCE MODEL FOR CLOTH

We consider cloth fabric as a mesh of interwoven cylinders oriented in two orthogonal directions. These cylinders, which we refer to as microcylinders, are considered to be very small compared to the geometry of the fabric. We define the scattering model from these microcylinders over the surface of the fabric similar to the

work by Marschner et al. [2005]. We use the gradient of texture UV coordinates of the mesh as the direction of microcylinders, but any other direction specification can be used. As discussed in section 4.3, we do not rely on a specific surface normal in our cylinder scattering model and therefore need only tangent directions at the cloth level (Section 5.1). However, the surface normal does come into play in shadowing/masking calculations (Section 5.2).

5.1 Shading Model

In order to render cloth fabrics, we evaluate the outgoing radiance from the *smallest patch* of the weaving pattern. This patch is the smallest portion of the weaving pattern which has the following property: the complete weave can be constructed by repeating this patch. Note that the smallest patch is not unique but all of them contain the same set of tangents (see Figure 12 left).

We assume that the smallest patch is locally flat and smaller than a pixel in the image plane. Additionally, for clarity, we constrain our discussion to cloth patches that contain exactly two threads, one orthogonal to the the other, as is common in most weaving patterns. However, the formulations in this section can be trivially extended to compute the contribution from any number of threads in a smallest patch. We define the outgoing radiance of the smallest patch to be the weighted average of the outgoing radiance of constituent threads based on their local orientation and coverage inside the smallest patch (See Figure 11):

$$L_r(\omega_r) = a_1 \times L_{r,1}(\omega_r) + a_2 \times L_{r,2}(\omega_r) \qquad (5)$$

where a_1 and a_2 represent the area coverage ratio of the first and second thread within the smallest patch respectively. If the weave pattern is watertight, these two numbers sum to one.

For each thread, we define a *tangent curve* that describes its tangent distribution inside the smallest patch (Figure 12 right). We specify the tangent curve by setting the tangent values at discrete control points. In order to compute the total radiance scattered by each thread, we sample its corresponding tangent curve and evalu-
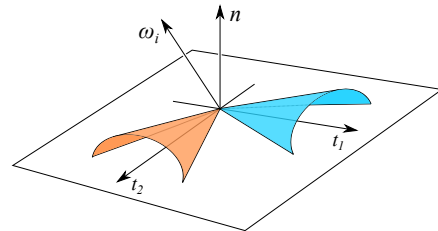

Fig. 11: Our shading model treats the fabric as a mesh of microcylinders oriented in two orthogonal directions.

ate the thread BRDF for each tangent direction j as:

$$L_{r,j}(\omega_r) = \frac{1}{N_j} \sum_t \int L_i(\omega_i) f_s(t, \omega_i, \omega_r) \cos\theta_i \, d\omega_i \quad (6)$$

where N_j is the number of tangent samples and f_s is the analytical thread BSDF model introduced in Section 4.3.
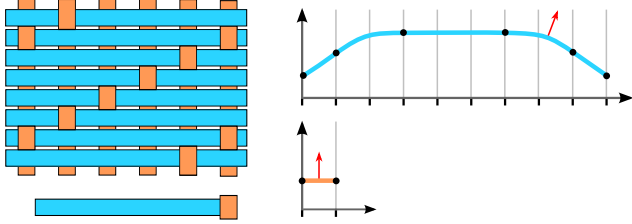

Fig. 12: The weaving pattern and a sample tangent curve for the Polyester Satin Charmeuse fabric: (left top) the weaving pattern, (left bottom) a smallest patch, (right) the tangent curve for the two types of threads. The red arrows indicate the local normal of the tangent.

5.2 Shadowing and Masking

Shadowing and masking are very important for the correct evaluation of the outgoing radiance especially at grazing angle viewing and lighting directions. Poulin and Fournier [1990] derived a shadowing and masking term for grooved surfaces composed of cylinders. However, their approach is not applicable to our model since they assumed that the cylinders have a surface patch BRDF and integrated all of the reflected light scattered toward a viewer. Since our formulation treats cylinders as one-dimensional entities, we do not compute the explicit reflectance variation across their circumference.

Shadowing and masking are very similar concepts; shadowing can be thought of as masking from the point of view of the light source. We interchangeably refer to both of these quantities as masking M in the rest of this section. We only compute the masking between the same types of threads (i.e. threads with the same cardinal directions). Shadowing between orthogonal threads is more involved and is left as future work.

Consider the setup shown in Figure 13 where the fabric is wrapped around a cylinder. Let us first focus on the horizontal threads only (Figure 13 middle). Threads along this direction never occlude each other from the viewer even at grazing angles. Therefore, the cylinder BSDF defined in Section 4.3 alone can be used to compute the correct outgoing radiance from these types of threads with no masking adjustment.

Now let us consider the vertical threads (Figure 13 right). At grazing angles each thread partially masks the thread behind it and gets masked by the thread in front of it. The amount of masking is relative to the cosine of the viewing direction projected to the thread normal plane and the surface normal. This angle is equal to ϕ_r (see Figure 9).

$$M(t, \omega_r) = \max(\cos\phi_r, 0) \quad (7)$$

If the cosine is negative, the surface is backfacing and is being self-masked. The same argument holds for the light direction and results in shadowing.

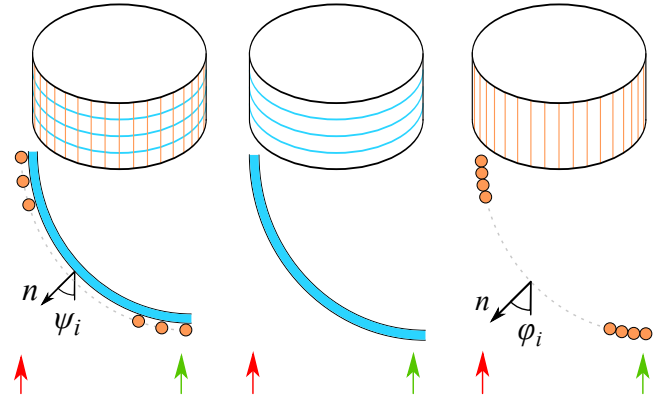$$M(t, \omega_i) = \max(\cos\phi_i, 0) \quad (8)$$

Fig. 13: Fabric as two different directions of threads with views from above (green arrows) and from grazing angles (red arrows): (left) The contribution of different threads in the smallest patch is related to the orientation of the patch. At grazing angles, the blue thread contributes less than the orange thread. (middle) In the longitudinal direction, there is no masking and no adjustment needed.(right) In the azimuthal direction, the amount of masking in grazing angles is dependent on the $\cos\phi_r$.

Here ϕ_i and ϕ_r are computed with respect to the local normal of the tangent t. If the tangent deviates from the surface tangent by α degrees then its normal will deviate from the surface normal by α degrees as well. See Figure 12 for an illustration.

When ω_i and ω_r are not correlated, the overall shadowing and masking amount is equal to the multiplication of $M(t, \omega_i)$ and $M(t, \omega_r)$. In cases where these two directions are close to each other, we use the adjustment introduced by Ashikhmin et al. [2000] to compute the overall shadowing and masking term $M(t, \omega_i, \omega_r)$:

$$M(t, \omega_i, \omega_r) = (1 - u(\phi_d)) \, M(t, \omega_i) \, \times \, M(t, \omega_r) + \\ u(\phi_d) \, \min(M(t, \omega_i), M(t, \omega_r)) \quad (9)$$

where u is a unit height Gaussian function with standard deviation between 15° and 25° [Ashikhmin et al. 2000]. We will refer to $M(t, \omega_i, \omega_r)$ in short as $M(t)$.

We can rewrite Equation 6 to include the effect of shadowing and masking:

$$L_{r,j}(\omega_r) = \frac{1}{N_j} \sum_t \int L_i(\omega_i) f_s(t, \omega_i, \omega_r) M(t) \cos\theta_i \, d\omega_i \quad (10)$$

To see the effect of shadowing and masking see Figure 15. Note the bright edges in the vertical mode which are the results of the contribution of all vertical flat fibers at grazing angles. The masking term corrects this effect by reducing the intensity of masked threads at grazing angles.

5.3 Reweighting

So far we have considered that the contribution of a thread to the overall reflection of the smallest patch is based on its length (i.e. area coverage). This is only correct when the ω_r and ω_i are near surface normal n. We need to adjust the contribution of each thread tangent t based on its projected length $P(t, \omega_i)$ in the direction of the viewer. Tangents that are more visible inside the smallest patch will have a higher contribution (for that viewing angle). We refer to this adjustment as reweighting. This process determines the contribution of each thread tangent curve sample to the overall reflectance of the smallest patch.

	η	Thread	A	k_d	γ_s	γ_v	a	Tangent Offsets (degrees)	Tangents Lenghts
(a)	1.46	Both	$(0.2, 0.8, 1) \times 0.3$	0.3	12	24	0.33	-25, 25	1
(b)	1.345	Flat	$(1, 0.95, 0.05) \times 0.12$	0.2	5	10	0.75	-35, -35, 35, 35	1, 1, 1
		Twisted	$(1, 0.95, 0.05) \times 0.16$	0.3	18	32	0.25	0, 0	1
(c)	1.539	Flat	$(1, 0.37, 0.3) \times 0.035$	0.1	2.5	5	0.9	-32, -32, -18, 0, 0, 18, 32, 32	1.33, 0.66, 2, 2, 0.66, 1.33
		Twisted	$(1, 0.37, 0.3) \times 0.2$	0.7	30	60	0.1	0, 0	1
(d)	1.539	Flat	$(1, 0.37, 0.3) \times 0.035$	0.1	2.5	5	0.67	-30, -30, 30, 30, -5, -5, 5, 5	1.33, 1.33, 1.33, 0, 0.67, 0.67, 0.67
		Twisted	$(1, 0.37, 0.3) \times 0.2$	0.7	30	60	0.33	0, 0	3
(e)	1.345	Dir 1	$(0.1, 1, 0.4) \times 0.2$	0.1	4	8	0.86	-25, -25, 25, 25	1.33, 2.67, 1.33
		Dir 2	$(1, 0, 0.1) \times 0.6$	0.1	5	10	0.14	0, 0	1
(f)	1.46	Dir 1	$(0.05, 0.02, 0) \times 0.3$	0.1	6	12	0.5	-90, -50	1
		Dir 2	$(0.05, 0.02, 0) \times 0.3$	0.1	6	12	0.5	-90, -55, 55, 90	0.5, 0, 0.5

Table II. : The list of parameters obtained from our measured cloth samples. The γ parameters are measured in degrees.
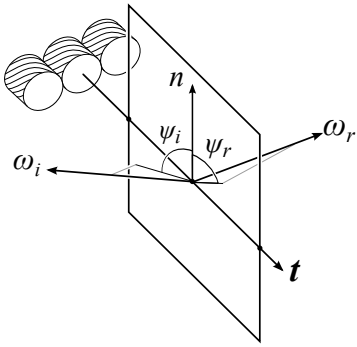
Fig. 14: Longitudinal angles ψ_i and ψ_r are the angles between local surface normal n and the projection of ω_i and ω_r on to the plane spanned by the t and n vectors.

Projection of the tangents onto the viewing direction is based on the cosine of the longitudinal angle ψ_r. As shown in Figure 14, ψ_r is the angle between local surface normal n and the projection of ω_r on to the plane that contains t and n.

$$P(t, \omega_r) = \max(\cos \psi_r, 0) \quad (11)$$

When the cosine is negative, the tangent is being self-masked and contributes zero to the overall reflection of the patch. Similar to the masking term, we calculate the projection for both ω_i and ω_r directions.

$$P(t, \omega_i) = \max(\cos \psi_i, 0) \quad (12)$$

This means that tangents receive energy based on their visibility from the point of view of the light source. We combine these two projections to get the final projection term $P(t, \omega_i, \omega_r)$:

$$P(t, \omega_i, \omega_r) = (1 - u(\psi_d)) \, P(t, \omega_i) \, \times \, P(t, \omega_r) + u(\psi_d) \, \min(P(t, \omega_i), P(t, \omega_r)) \quad (13)$$

where ψ_d is the difference between ψ_i and ψ_r. We refer to $P(t, \omega_i, \omega_r)$ in short as $P(t)$. Finally we can rewrite Equation 10 and put it in Equation 5 to get the final outgoing radiance of the smallest patch:

$$L_{r,j}(\omega_r) = \frac{1}{Q} \frac{1}{N_j} \sum_t \int L_i(\omega_i) f_s(t, \omega_i, \omega_r) M(t) P(t) \cos \theta_i \, d\omega_i \quad (14)$$

Here Q is a normalization factor computed as:

$$Q = \frac{a_1}{N_1} \sum_t P(t) + \frac{a_2}{N_2} \sum_t P(t) + (1 - a_1 - a_2)(\omega_r \cdot n) \quad (15)$$

where N_1 and N_2 are the number of samples of each thread direction, and n is the surface normal of the fabric. The last component in this equation accounts for the projected area of the gaps in the case the threads do not cover the patch completely (e.g. the Linen Plain fabric) and $a_1 + a_2 < 1$. The reweighting adjustment in Equation 14 reduces the contribution of foreshortened threads in the smallest patch which is especially important for grazing angles. The effect of reweighting on the final result is demonstrated in Figure 15. In the vertical mode, the flat threads contribute more to the final radiance than the twisted threads since they occupy more area of the projected smallest patch.
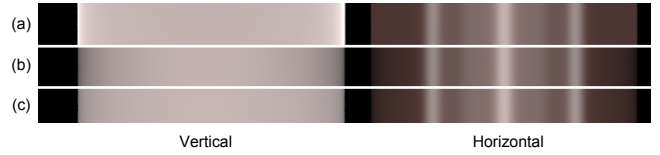

Fig. 15: The effect of shadowing and masking and the reweighting process on the final results: (a) the result for the shading model, (b) the effect of shadowing/masking term, and (c) the final results after applying shadowing/masking and reweighting.

6. RESULTS

We have implemented the cloth model in a ray tracer and on the GPU. This section contains rendered results for several different cloth fabrics. The parameters for each cloth sample are summarized in Table II.

We validate our cloth model by comparing rendered results to photographs. To capture the anisotropic behavior of different fabrics, we wrapped the fabrics around a cylinder in three different directions. We label each mode based on the orientation of the flat threads as vertical, horizontal, and diagonal (see Figure 16). For the Linen Plain fabric, the vertical and horizontal modes are identical. For comparison, we present our rendered results of different fabrics in the same setup. Figure 17 shows Linen Plain fabric. The top row images are the photographs of the fabric and the bottom row images are rendered using our model. The graphs show the average values of the pixels on the y-axis. This fabric shows similar
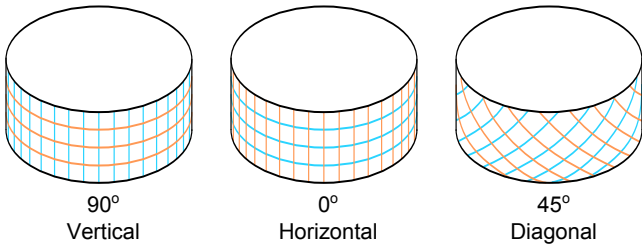
Fig. 16: To capture the anisotropic behavior of different fabrics, we have wrapped the fabric around a cylinder in three different orientations where the flat threads stay (left) vertical, (middle) horizontal, and (c) diagonal.

behavior on the vertical and horizontal mode due to the symmetry of the plain weaving pattern. However, it has a different appearance when the sample is rotated 45 degrees in the diagonal mode, which demonstrates the subtle anisotropic behavior of this fabric. Our renderings qualitatively match the photographs in all three cases. Figure 18 shows the results for the Silk Crepe de Chine
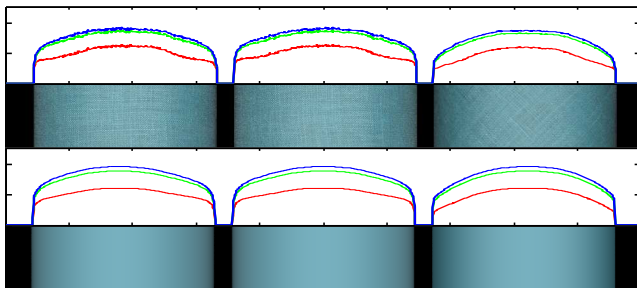

Fig. 17: Photograph (top row) and the rendered result (bottom row) of the Linen Plain fabric. Thread tangent curves for the warp and weft are pictured at (right).

fabric. This fabric has grazing angle highlights in the vertical mode and shows two off-specular highlights in the horizontal mode. The two off-specular peaks are due to the two constant slope segments inside the tangent distribution of the flat threads (shown in blue). These behaviors can be seen in the BRDF measurements of this fabric as well (see Figure 5). However, it is important to note that these plots are essentially different; in the BRDF measurements, the ω_i and surface normal n are fixed and the ω_r is changing, while in these graphs the ω_i and ω_r are fixed and n is changing. Our model can successfully capture the light scattering behavior of this fabric under all three orientations. The photograph and the renderings
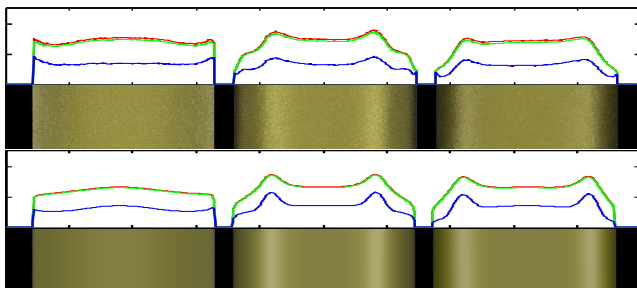

Fig. 18: Photograph (top row) and the rendered result (bottom row) of the Silk Crepe de Chine fabric. Thread tangent curves for the warp and weft are pictured at (right).

for the front side of Polyester Satin Charmeuse fabric are shown in Figure 19. The back side of this fabric shown in Figure 20 has a different appearance due to the asymmetry of the weaving pattern. On the front side, the fabric has a flat appearance in the vertical mode and presents three sharp specular highlights in the horizontal mode. These three highlights are due to the three constant slope segments inside the tangent distribution of the flat threads (shown in blue) in the weaving pattern. On the back side, we can see four highlights in the horizontal mode. Our renderings reproduce the appearance of this fabric for both sides and for all three orientations with the same parameters. Figure 21 shows a comparison of our
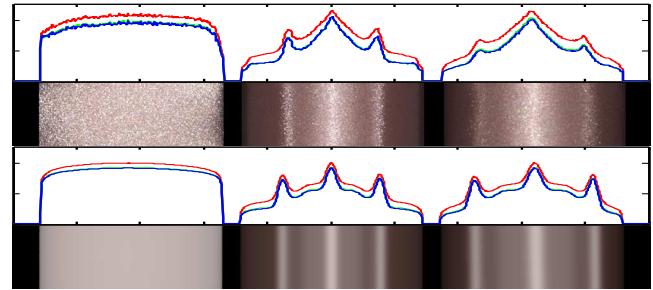

Fig. 19: Photograph (top row) and the rendered result (bottom row) of the front-side of Polyester Satin Charmeuse fabric. Thread tangent curves for the warp and weft are pictured at (right).
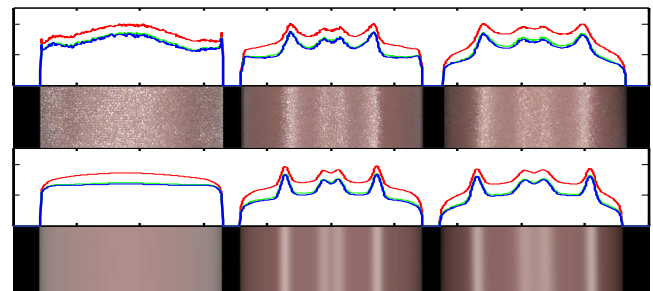

Fig. 20: Photograph (top row) and the rendered result (bottom row) of the back-side of Polyester Satin Charmeuse fabric. Thread tangent curves for the warp and weft are pictured at (right).

model BRDF with the measured BRDF of the fabric (Figure 21 top) for the front side of the fabric and along the direction of flat threads. Note, how our model is able to capture the variation in the location of the highlights and the overall shape of the reflected light as the light source moves from normal incidence to 30 and 60 degrees. Figure 22 demonstrates how our model can reproduce the appearance of other fabrics that have been previously studied. We have successfully matched a Silk Shot fabric presented in [Pont and Koenderink 2003] (Figure 22) and a Velvet fabric presented in [Ashikhmin 2001] (Figure 23). The Silk Shot fabric is composed of threads with two different colors (in this case red and green) resulting in a complex anisotropic appearance. Our model can reproduce this appearance using anisotropic volume scattering by the colored threads rather than the shadowing and masking effect as it was assumed by Pont and Koenderink [Pont and Koenderink 2003]. Figure 23 shows how asymmetric highlights of Velvet can be repro-
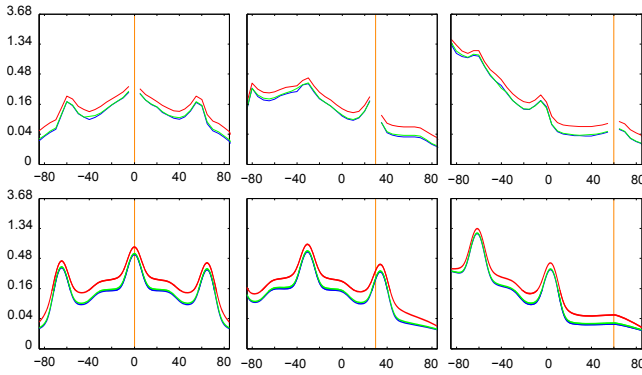
Fig. 21: Matching a BRDF measurement of the Polyester Satin Charmeuse fabric with our model. (top) normal plane BRDF measurement of the front side of Polyester Satin Charmeuse fabric along the direction of flat threads compared to (bottom) the result of our appearance model.

Fig. 22: Photographs (top row) and rendered samples (bottom row) of a Silk Shot Fabric (from [Pont and Koenderink 2003]). Thread tangent curves pictured at (right).

duced by setting the tangent curves to be near perpendicular to the surface of the fabric. Figure 24 shows a variety of fabrics using

Fig. 23: Photographs (top row) and rendered samples (bottom row) for Velvet Fabric (from [Ashikhmin 2001]). Note that our model can successfully reproduce the asymmetric highlights seen in the horizontal mode. Thread tangent curves pictured at (right).

our model. In this image we are using a texture map to specify the groom direction for the Velvet fabric. We also included two imaginary fabrics: one is a weaving of silk and polyester threads using a Shantung weaving pattern and the other is using an imaginary fabric with asymmetric specular peaks.

In order to reproduce the appearance of new fabrics, users can take advantage of our thread BSDF parameters as a starting point without the need for any measurements. We have presented several BSDFs for common thread types which establish parametric constraints for existing materials. By observing with the naked eye or a macro lens, one can approximate the weave pattern and define the tangent curves. Alternatively, one can guess the weaving structure and thread BSDF by investigating the overall cloth appearance (e.g. from our cylinder setup).

6.1   Performance

The images in Figure 24 of a piece of cloth illuminated by an area light have been rendered in 512×512 resolution with 144 samples per pixel in an unoptimized CPU ray tracer. For The renderings took 51 minutes on average on an 2.83 GHz Intel Core 2 CPU.

We also implemented the full cloth model in a GPU shader. The images in Figure 25 are lit by a single directional light and were rendered in 100 ms for 1 sample per pixel on a laptop with an Intel I5 M480 processor and a mobile NVIDIA GT420 GPU. There is a host of performance optimizations available to our algorithm specifically in the areas of precomputed lookup tables and tangent curve sampling. We aim to address this in future work as we extend the capabilities of this model.

Fig. 25: Screenshots from the GPU implementation of our model under a single directional lighting. Each image was rendered in roughly 100 ms on a mobile GT420 GPU.

7.   DISCUSSION

As shown in the results, our model is able to reproduce the complex behavior of a variety of fabrics. Our appearance model is based on an analytical thread BSDF and a tangent distribution to describe a weaving pattern. Our work is similar to the model of Ashikhmin et al. [2000] since it can reproduce specular highlights in any direction. We accomplish this by orienting the thread tangents so that their reflection cone lies in the desired direction. The input of our model is intuitively based on the weaving pattern of the fabric, while the microfacet model requires a complicated mathematical representation of the facet normals. For example, to produce the appearance of Velvet, Ashikhmin et al. propose $c \times \exp(-\cot^2 \theta / \sigma^2)$ as the normal distribution (where c and σ are control parameters). Formulating such an equation can be a challenging task. In our model, we represent Velvet by simply defining the thread tangents to be nearly parallel to the surface normal.

State of the art research in cloth rendering has been carried out by Irawan and Marschner [2012]. They present a rigorous model for computing light reflection off of yarn threads, which are simulated as an assembly of specular fibers. The model incorporates costly numerical integrations and a fitting process to estimate the value of different control parameters. We implemented the Irawan cloth BRDF as a shader in PBRT for comparison purposes. Irawan's model is capable of reproducing a range of appearances including Linen Plain and Silk Crepe de Chine as seen in Figure 26. Irawan's model can reproduce the appearance of Linen Plain fabric relatively well, but fails to reproduce the grazing angle highlights seen in the vertical mode of the Silk Crepe de Chine fabric. One of the limitations of Irawan's model is that the curvature of the threads has to be a hyperbolic curve. This constraint is a core component of the Irawan model because it simplifies the computation of the complex lighting integrals that are involved. Because of this limitation, Irawan's model can produce only one highlight (for large positive values of κ) or two very sharp highlights (for values of κ close to -1). Consequently, Irawan's model cannot reproduce all the highlights seen in the Polyester Satin Charmeuse fabric (Figure 27). For both sides of this fabric, Irawan's model is unable to produce more than two highlights. We present two sets of rendered images for each side, in order to match two of the highlights at a time. The

Fig. 24: Our rendered results for different fabrics lit by a square area light. From top to bottom, left to right: Linen Plain, Silk Crepe de Chine, front side of Polyester Satin Charmeuse, back side of the Polyester Satin Charmeuse, Silk Shot Fabric, Velvet, an imaginary fabric made out of silk and polyester threads with a Shantung weaving pattern, and an imaginary fabric with asymmetric specular peaks.
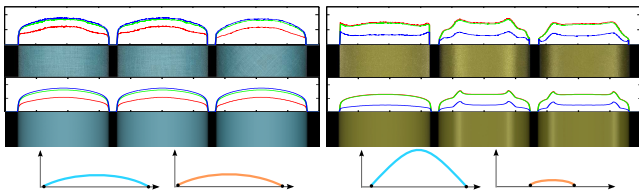

Fig. 26: Photographs (top row) and the rendered results (bottom row) using Irawan's model for the (left) Linen Plain fabric and (right) Silk Crepe de Chine fabric. Note that this model is unable to reproduce grazing angle highlights seen in the vertical mode in the Silk Crepe de Chine fabric.
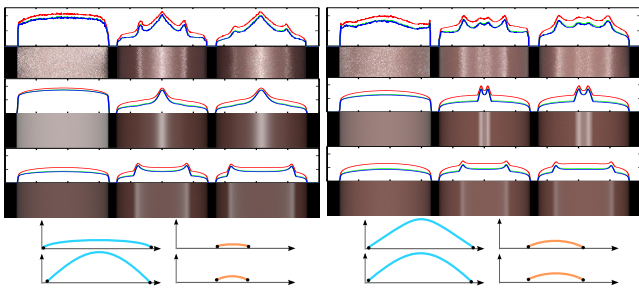

Fig. 27: Photographs (top row) and two rendered results (middle and bottom rows) by Irawan's model for the (left) front-side and (right) back-side of the Polyester Satin Charmeuse fabric. Note that this model cannot reproduce more than two highlights in all cases and fails to reproduce the correct appearance.
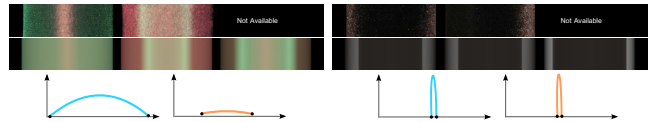

Fig. 28: Photograph (top row) and the rendered results (bottom row) using Irawan's model for the (left) Shot fabric and (right) velvet. In order to match the Shot fabric we had to multiply the specular component with a color value. Also, note that this model fails to reproduce the asymmetric highlights of velvet.

coefficient k_s with different color values, which is physically incorrect due to the fact that simple surface reflection maintains the color of the incident light. Choosing two different k_d colored values (red and green) resulted in a brown mixture of both colors in all three orientations.

Additionally, hyperbolic curves cannot represent constant slope segments and therefore the off-specular highlights in the Irawan model are very sharp and narrow. To alleviate this problem, Irawan et al. use a smoothstep function which softens outside of the highlights, but also produces the undesired artifact of a sharp transition at the start of highlights (see the results for Velvet in Figure 28). The smoothstep function aside from lacking a physical basis, also alters the position of the highlights and makes the model less predictable. Finally, Irawan's model does not account for shadowing and masking between threads. We have summarized all of the parameters of the Irawan model used for rendering different fabrics in the supplemental material.

A limitation of our model in its current form is that it cannot accurately produce close-up renderings. It does not reproduce the appearance of single threads in a patch, or the reflectance variation across each thread. This limitation can be somewhat worked around with a texture, but a texture will fail for extreme close-ups, where it will be necessary to model actual geometry such as [Zhao

symmetry of hyperbolic curves also makes it impossible to reproduce the asymmetric highlights seen in the Velvet fabric (See Figure 28). The Silk Shot fabric is also a challenge for Irawan's model. In order to match the measurement we had to multiply the specular

et al. 2011]. Additionally, our shadowing and masking term does not handle masking between threads in orthogonal directions. This causes an underestimation of masking at extreme grazing angles. Finally, our model ignores the effect of multiple scattering between different threads.

8. CONCLUSION AND FUTURE WORK

We have presented a practical appearance model for cloth fabrics. Our model is robust and easy to use, while being able to reproduce the complex anisotropic appearance of cloth. We present both measurements and a novel scattering model for threads. Our cloth BRDF is based on the distribution of thread tangents, and it includes shadowing and masking terms that are important for grazing angle viewing and lighting. Our results show that we can match the appearance of real fabrics including reproducing the complex anisotropic highlights and color shifts. We also demonstrate how previous state-of-the-art models for cloth appearance fail to reproduce important scattering phenomena that are common in fabrics.

One avenue for future research is investigating the shadowing and masking between threads with different directions. Additionally, we are interested in testing automated fitting processes to estimate the parameters of our model based on photographs of a fabric wrapped around a cylinder in different directions. Furthermore, we aim to investigate the transmission term and approximate the multiple scattering of light between different threads. Lastly, it would be interesting to investigate different ways of importance sampling our fabric BRDF.

9. ACKNOWLEDGMENTS

REFERENCES

ADABALA, N., MAGNENAT-THALMANN, N., AND FEI, G. 2003. Visualization of woven cloth. In *Proceedings of the 14th Eurographics workshop on Rendering*. EGRW '03. Eurographics Association, Aire-la-Ville, Switzerland, Switzerland, 178–185.

ASHIKHMIN, M., PREMOŽE, S., AND SHIRLEY, P. 2000. A microfacet-based brdf generator. In *Proceedings of the 27th annual conference on Computer graphics and interactive techniques*. SIGGRAPH '00. ACM Press/Addison-Wesley Publishing Co., New York, NY, USA, 65–74.

ASHIKHMIN, M. V. 2001. Approximate methods for improving surface appearance. Ph.D. thesis. AAI3012256.

CHANDRASEKHAR, S. 1960. *Radiative Transfer*. Dover Publications.

CHEN, Y., LIN, S., ZHONG, H., XU, Y.-Q., GUO, B., AND SHUM, H.-Y. 2003. Realistic rendering and animation of knitwear. *IEEE Transactions on Visualization and Computer Graphics 9,* 1, 43–55.

DAUBERT, K., LENSCH, H. P. A., HEIDRICH, W., AND SEIDEL, H.-P. 2001. Efficient cloth modeling and rendering. In *Proceedings of the 12th Eurographics Workshop on Rendering Techniques*. Springer-Verlag, London, UK, 63–70.

DRAGO, F. AND CHIBA, N. 2004. Painting canvas synthesis. *Vis. Comput. 20,* 5, 314–328.

GLUMAC, R. AND DOEPP, D. 2004. Generalized approach to rendering fabric. In *ACM SIGGRAPH 2004 Sketches*. SIGGRAPH '04. ACM, New York, NY, USA, 120–.

HANRAHAN, P. AND KRUEGER, W. 1993. Reflection from layered surfaces due to subsurface scattering. In *Proceedings of the 20th annual conference on Computer graphics and interactive techniques*. SIGGRAPH '93. ACM, New York, NY, USA, 165–174.

IRAWAN, P. AND MARSCHNER, S. 2012. Specular reflection from woven cloth. *ACM Trans. Graph. 31,* 1 (Feb.), 11:1–11:20.

JAKOB, W., ARBREE, A., MOON, J. T., BALA, K., AND MARSCHNER, S. 2010. A radiative transfer framework for rendering materials with anisotropic structure. *ACM Trans. Graph. 29,* 53:1–53:13.

KAJIYA, J. T. AND KAY, T. L. 1989. Rendering Fur With Three Dimensional Textures. In *Computer Graphics (Proceedings of SIGGRAPH 89)*. ACM, New York, NY, USA, 271–280.

KIM, T.-Y. 2002. Modeling, Rendering and Animating Human Hair. Ph.D. thesis, University of Southern California, Los Angeles, CA, USA.

MARSCHNER, S. R., JENSEN, H. W., CAMMARANO, M., WORLEY, S., AND HANRAHAN, P. 2003. Light Scattering from Human Hair Fibers. *ACM Transactions on Graphics 22,* 3, 780–791.

MARSCHNER, S. R., WESTIN, S. H., ARBREE, A., AND MOON, J. T. 2005. Measuring and modeling the appearance of finished wood. *ACM Trans. Graph. 24,* 3 (July), 727–734.

PONT, S. C. AND KOENDERINK, J. J. 2003. Split off-specular reflection and surface scattering from woven materials. *Appl Opt 42,* 8, 1526–33.

POULIN, P. AND FOURNIER, A. 1990. A model for anisotropic reflection. In *Proceedings of the 17th annual conference on Computer graphics and interactive techniques*. SIGGRAPH '90. ACM, New York, NY, USA, 273–282.

SADEGHI, I., PRITCHETT, H., JENSEN, H. W., AND TAMSTORF, R. 2010. An artist friendly hair shading system. *ACM Trans. Graph. 29,* 56:1–56:10.

SAVILLE, B. P. 1999. *Physical Testing of Textiles*. CRC Press.

SCHRÖDER, K., KLEIN, R., AND ZINKE, A. 2011. A volumetric approach to predictive rendering of fabrics. *Computer Graphics Forum (Proceedings of EGSR 2011) 30,* 4 (July), 1277–1286.

WANG, J., ZHAO, S., TONG, X., SNYDER, J., AND GUO, B. 2008. Modeling anisotropic surface reflectance with example-based microfacet synthesis. In *ACM SIGGRAPH 2008 papers*. SIGGRAPH '08. ACM, New York, NY, USA, 41:1–41:9.

WEIL, J. 1986. The synthesis of cloth objects. In *Proceedings of the 13th annual conference on Computer graphics and interactive techniques*. SIGGRAPH '86. ACM, New York, NY, USA, 49–54.

WESTIN, S. H., ARVO, J. R., AND TORRANCE, K. E. 1992. Predicting reflectance functions from complex surfaces. *SIGGRAPH Comput. Graph. 26,* 2, 255–264.

XU, Y.-Q., CHEN, Y., LIN, S., ZHONG, H., WU, E., GUO, B., AND SHUM, H.-Y. 2001. Photorealistic rendering of knitwear using the lumislice. In *Proceedings of the 28th annual conference on Computer graphics and interactive techniques*. SIGGRAPH '01. ACM, New York, NY, USA, 391–398.

YANG, L. 2009. Cse 348b final project: Cloth rendering. https://graphics.stanford.edu/wikis/cs348b-09/lfyg/Final_Project_Writeup/.

YASUDA, T., YOKOI, S., TORIWAKI, J.-I., AND INAGAKI, K. 1992. A shading model for cloth objects. *IEEE Comput. Graph. Appl. 12,* 15–24.

Zhao, S., Jakob, W., Marschner, S., and Bala, K. 2011. Building volumetric appearance models of fabric using micro ct imaging. *ACM Trans. Graph.*.

Supplemental Material

Parameters used to produce the rendered results of the Irawan's model for (a) Linen Plain, (b) Silk Crepe de Chine, (c_1) inner highlights of the front-face of Polyester Satin Charmeuse, (c_2) outer highlights of the front-face of Polyester Satin Charmeuse, (d_1) inner highlights of the back-face of Polyester Satin Charmeuse, (d_2) outer highlights of the back-face of Polyester Satin Charmeuse, (e) Silk Shot fabric, and (f) Velvet.
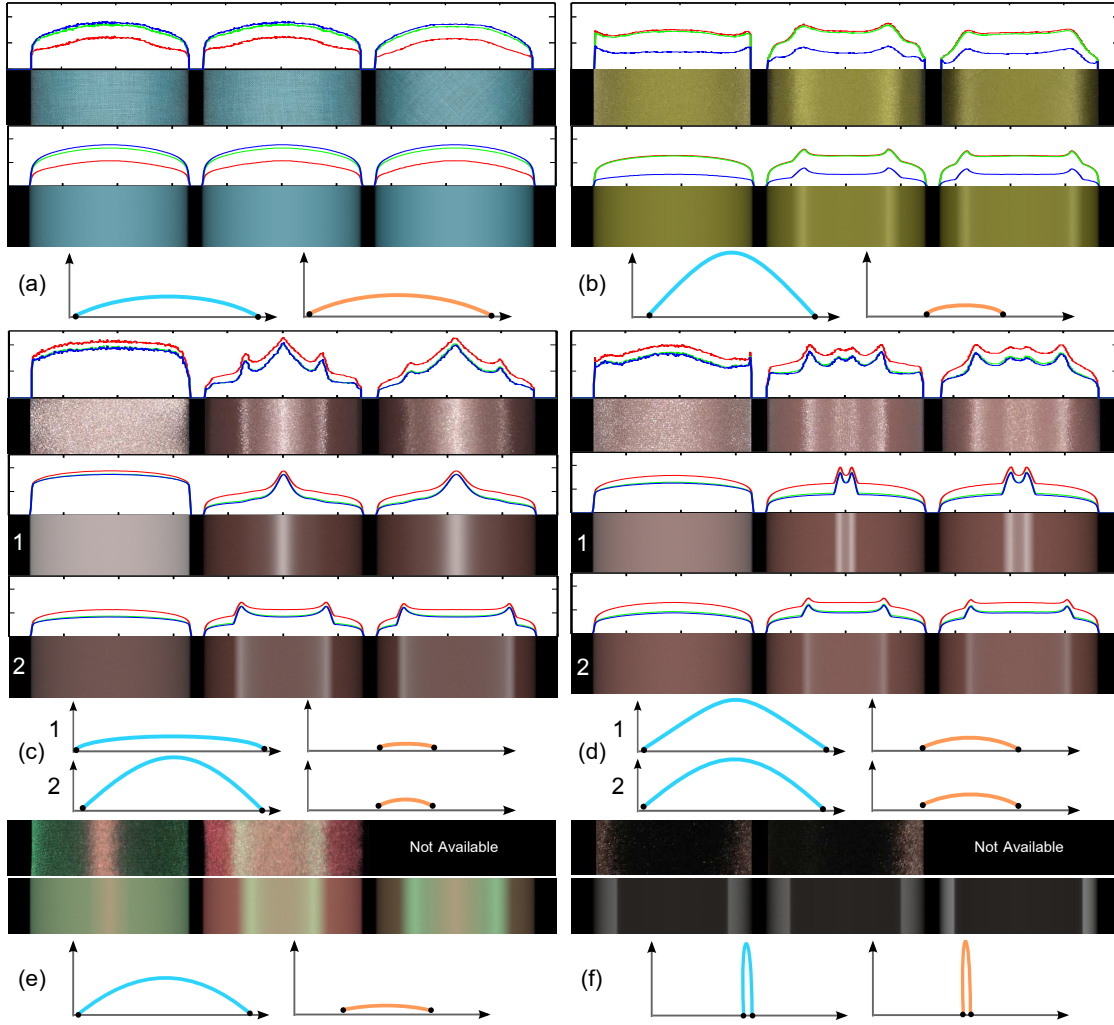
Fabric	Thread	Type	k_d	k_s	α	β	δ	Ψ	U_{max}	κ	w	l
(a)	both	staple	$(0.2, 0.8, 1) \times 0.09$	$(1, 1, 1) \times 0.7$	0.01	6	0.0	20	25	0.0	1.0	1.0
(b)	warp	filament	$(1, 0.95, 0.05) \times 0.48$	$(1.36, 1.312, 0.448)$	0.1	10	0.3	0	45	-0.9	1.0	2.0
	weft	staple	$(1, 0.95, 0.05) \times 0.48$	$(1, 1, 1)$	0.1	4	0	30	45	1.0	1.0	1.0
(c_1)	warp	filament	$(1, 0.37, 0.3) \times 0.0035$	$(1, 1, 1) \times 0.9$	0.01	8	0.5	0	35	2.0	1.0	4.0
	weft	staple	$(1, 0.37, 0.3) \times 0.14$	$(1, 1, 1) \times 0.3$	0.01	2	0.0	30	25	0.0	1.0	1.0
(c_2)	warp	filament	$(1, 0.37, 0.3) \times 0.0035$	$(1, 1, 1) \times 0.9$	0.01	8	0.2	0	40	-0.85	1.0	4.0
	weft	staple	$(1, 0.37, 0.3) \times 0.14$	$(1, 1, 1) \times 0.3$	0.01	2	0.0	30	25	0.0	1.0	1.0
(d_1)	warp	filament	$(1, 0.37, 0.3) \times 0.0035$	$(1, 1, 1) \times 0.9$	0.01	4	0.6	0	9	-0.7	1.0	2.0
	weft	staple	$(1, 0.37, 0.3) \times 0.14$	$(1, 1, 1) \times 0.3$	0.01	2	0.0	30	25	0.0	1.0	1.0
(d_2)	warp	filament	$(1, 0.37, 0.3) \times 0.0035$	$(1, 1, 1) \times 0.9$	0.01	10	0.2	0	35	-0.9	1.0	2.0
	weft	staple	$(1, 0.37, 0.3) \times 0.14$	$(1, 1, 1) \times 0.3$	0.01	2	0.0	30	25	0.0	1.0	1.0
(e)	warp	filament	$(0.1, 1, 0.4) \times 0.04$	$(0.7, 2.5, 1.3)$	0.01	40	0.4	0	37	-0.7	1.0	2.0
	weft	filament	$(1, 0, 0.1) \times 0.12$	$(2.3, 0.3, 0.5)$	0.01	40	0.2	0	15	1.0	1.0	1.0
(f)	both	filament	$(0.05, 0.02, 0) \times 0.03$	$(1, 1, 1) \times 0.9$	0.0	10	0.5	0	90	-0.99	1.0	1.0